Journal of Mining and Environment (JME), Vol. 14, No. 4, 2023, 1061-1079

Shahrood University of Technology

Journal of Mining and Environment (JME)

Journal homepage: www.jme.shahroodut.ac.ir

Iranian Society of Mining Engineering (IRSME)

Hydrogeophysical Survey for Assessment of Groundwater Budget and Aquifer Protection in Hilly Terrain

Sonu Singh[1]*, Vijay Shankar[1], and Joseph Tripura[2]

1. Department of Civil Engineering, National Institute of Technology Hamirpur, India
2. Department of Civil Engineering, National Institute of Technology Patna, India

Article Info

Received 9 March 2023
Received in Revised form 6 July 2023
Accepted 17 July 2023
Published online 17 July 2023

DOI: 10.22044/jme.2023.12816.2329

Keywords

VES
Hydraulic parameters
Geoelectrical data
Aquifer protective capacity
Hilly terrain

Abstract

Assessing the groundwater potential (GWP) and protective capacity of aquifers is essential to provide solutions to challenges in aquifer exploration and conditions in hilly terrain regions. The study was conducted in the hilly terrain region of Hamirpur, Himachal Pradesh, India, to obtain one-dimensional vertical electrical sounding (VES) data for groundwater exploration and evaluate the vulnerability of sublayers. Forty VES sites were used in the Schlumberger electrode configuration. The analysis of data resulted in stratified 2-5 different curves. According to the geoelectric sections, there are two to five layers of soil beneath the region i.e. Shale/clay (10-650 Ohm-m), fractured sandstone/gravel/sand (10.3-436 Ohm-m), clay mix gravel/clay mix sand/coarse-grained sandstones (1.06-355 Ohm-m), conglomerate/clay/hard sandstone (60.5-658.7 Ohm-m), sandstone/shale (90.8-125 Ohm-m) with aquifer resistivity (AR) in parenthesis. Aquifer resistivity (AR), longitudinal conductance (S), layer thickness (LT), and transverse resistivity (TR) distribution maps were generated using interpreted VES data for various sub-layers using ArcGIS 10.1. The geologic second and third sub-surface layers are generally porous and permeable. S values for underlying layers are generally less than unity, which indicates vulnerable zones with a significant risk of contamination. Based on the S values, the strata are divided into five categories as Poor (5.55%), weak (19.43%), moderate (19.45%), good (38.89%), and very good (16.68%). Areas with moderate to very good protection capacity are planned as zones with high GWP. The study results are useful in preliminary pollution control and assessment for sustainable groundwater management.

1. Introduction

Groundwater is the primary source of drinking water for almost 2.5 billion people globally [1]. In many farming locations, groundwater withdrawal has significantly aided social and economic development, improved food security, and reduced the effect of drought [2-4]. Groundwater abstraction can mitigate the short-term effects of drought on agriculture and domestic water supplies [5]. The rapid decrease of water levels can be an unintended consequence of humanity's reliance on groundwater [6-8], and leads to water quality degradation [9-12]. The indiscriminate sinking of boreholes does not consider the site's prior geophysical, hydrogeological, and geological investigations. This attributes to the temporary functioning of boreholes and results in a very low success rate of the boreholes [13]. Knowledge of the fundamental characteristics of the aquifer is required for groundwater exploration including the determination of natural flow, bedrock depth, and groundwater availability in terms of quality and quantity [14]. Some traditional methods such as test hole drilling and log analysis are employed to characterize the protective layer thickness and lateral extent but have limitations of cost and input effort [15]. Hence, the deep study of groundwater exploration techniques is essential to overcome these limitations.

Electrical resistivity has been used in a variety of geophysical investigations including mineral

✉ *Corresponding author: sonu@nith.ac.in (S. Singh)*

exploration [16-26], engineering investigations [27-29], geothermal studies [30-32], archaeological surveys [33-36], geological mapping [37-40], and groundwater monitoring [41]. It is critical to define groundwater potential zones in order to assess a region's groundwater potential [42]. Furthermore, appropriately managing groundwater resources is enhanced by properly describing suitable groundwater potential zones [43-46], which requires a detailed examination of sites selection for groundwater abstraction. Among several geo-physical techniques used to study sub-surface properties, the commonest is VES to delineate the most suitable area for groundwater exploration [47, 48]. It is inferred, on the basis of numerous case studies, that the application of VES is successful in groundwater exploration.

However, in addition to the challenges in identifying potential groundwater bodies, many researchers have also investigated the nature of aquifer protection. Shailaja *et al.* [49] examined aquifer protection in Maharashtra, India, a higher drought region, using vertical electrical sounding in the Schlumberger electrode configuration. The study region has few aquifers in the horizontal, vertical extent, and are available at greater depth pertaining to the hilly terrain. Water demand there is high necessitating the need for groundwater exploration. The data from drilling reflects substantial variation in water table depth in the aquifers of the study area [50]. Table 1 gives the water table data of the studied area.

Although the hydro-geophysical surveys have been done in many parts of the world to evaluate groundwater reserves and aquifer protection, most of the studies are primarily focused on the general aspects of the aquifer system or the investigations on the most protective layer for aquifer protection.

Literature indicates that very few studies have been conducted to assess groundwater budget and aquifer protection with a comprehensive assessment of all the subsurface layers. The present study investigates the characteristics of all the subsurface layers (including resistivity parameters) through the hydro-geophysical survey, thus comprehensively assessing all subsurface layers to identify groundwater reserves and protection. The specific objectives of the current study are (i) Evaluating aquifer protective capacity and providing adequate recommendations for the groundwater abstraction and (ii) Asse ssing the groundwater budget, aquifer protection, and vulnerability of the sub-surface layers through a hydro-geophysical survey.

2. Materials and Methods

2.1. Location and geology of studied area

The studied area, i.e. Hamirpur, is in the Indian state of Himachal Pradesh, and is bounded by latitudes 31°24' 48" to 31°53'35" and longitudes 76°17'50" to 76°43'42" (Figure 1). It is covered by the far northern high-altitude Dhauladhar ranges and is characterized as hilly terrain. The proposed studied area is primarily based on a homogenized soil-water interaction. Knowledge of soil-water interaction is a key essential in solving several real-world problems encountered in different engineering projects such as soil erosions, soil stabilization, leaching of pollutants, potential groundwater zone delineation, aquifer characteristics identification, etc. The studied area covers only 1118 square kilometres (2.01% of the state's total area). The study region has the highest population density with 406 people per square kilometer in the state of Himachal Pradesh [51]. Hamirpur, Badsar, Bhoranj, Nadaun, and Sujanpur are the administrative units of studied area [52].

Seasonal conditions are differentiated into three broad categories, i.e. October to March as winters, April to June as summers, and monsoon from July to September. Hamirpur experiences moderate rainfall, with maximum precipitation in July and August. According to Central Groundwater Board CGWB [52], Hamirpur receives 1340.72 mm as average annual rainfall, of which June to September record about 82%. The River Beas drains the area, with the tributaries Maan Khad and Kunah Khad running on each side. Minimum and maximum temperatures typically vary from 3 °C to 35 °C.

The studied area is classified into different regions based on Siwalik groups i.e. upper Siwalik, middle Siwalik, and lower Siwalik, for the development of groundwater. The lower, middle and upper Shiwalik group makes up the region's geology (Figure 2). Dark gray sandstone and purple shales in lower Shiwaliks, and are overlain by grey clay and micaceous sandstone. The upper Shiwaliks are composed of conglomerates, coarse-grained sandstones, and beds of sandstone or pebbles interbedded with grey and pink clays and silts. The northern part of the district is underlain by hard and compact conglomerates, whereas weathered and fractured conglomerate found in the southern region.

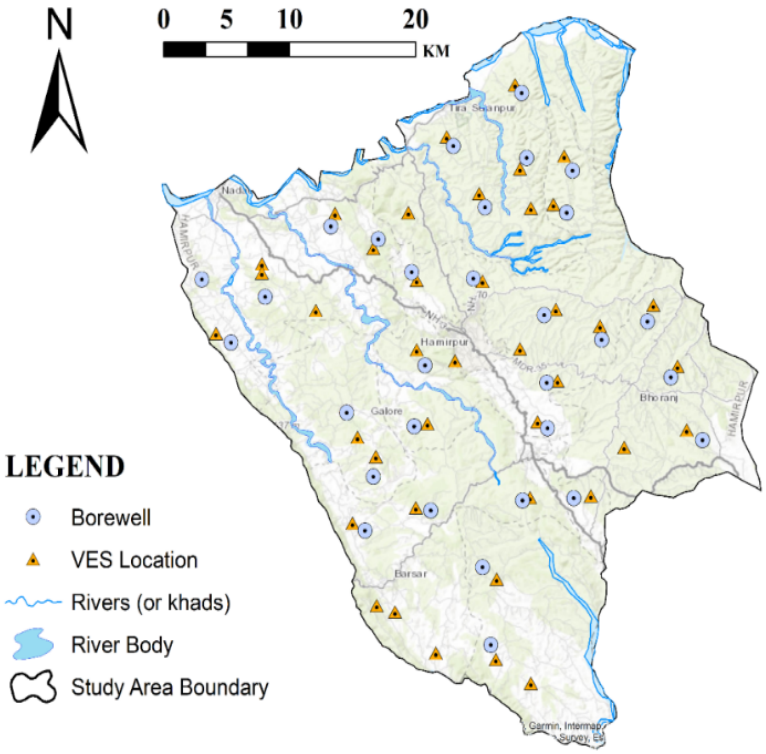

Figure 1. Studied area map.

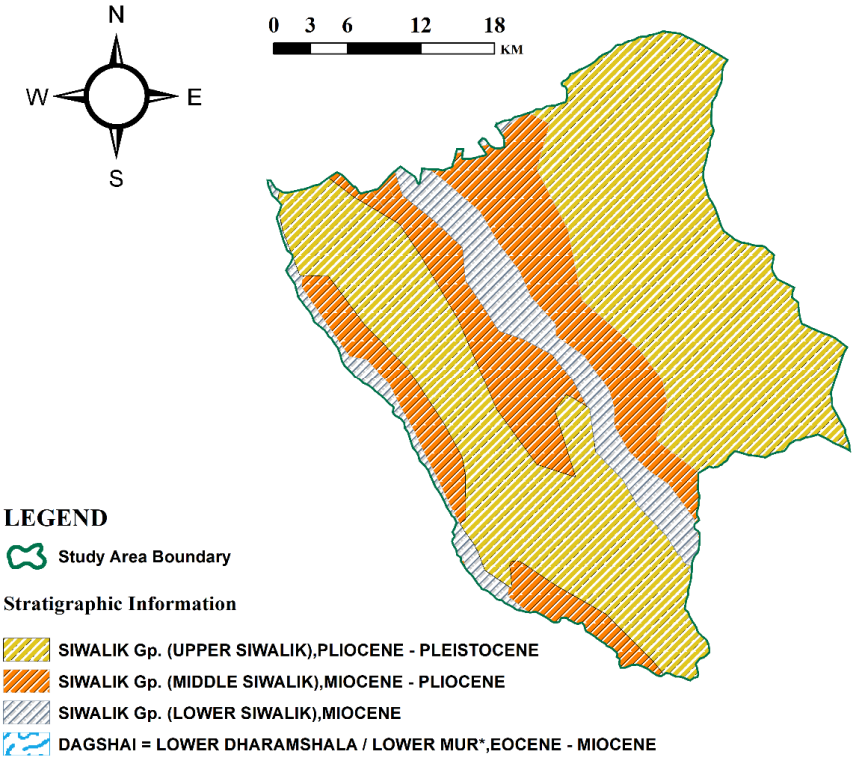

Figure 2. Geological map of the studied area.

2.2. Designing geo-physical surveying

The signal stacking-based signal enhancement resistivity meter (Model: SSR-MP-AT) has been used for VES measurement for field survey in the studied area. The instrument is a reliable geo-physical tool that provides high-quality measurements since it includes many novel features and cutting-edge digital circuit technology. The ration for the signal and noise of the device can be enhanced for non-coherent earth noises by increasing the number of stacks. The device is an innovative geophysical tool with digital circuitry techniques that ensure precise readings. The instrument in action during a field survey is shown in Figure 3. The apparent resistivity is measured directly. The distance between potential electrodes and current electrodes were entered using the resistivity meter's built-in keypad to calculate apparent resistivity. The arrangement of Schlumberger is shown in Figure 4. The current electrodes are represented by M and N, whereas the potential electrodes are represented by A and B. The space between the current electrodes is kept as wide as possible to better analyze the sub-surface properties at greater depths. To examine the geo-physical survey, the vertical electrical sounding (VES) test at 40 sites used a maximum half current electrode spacing (MN/2) of 350 m. All stations' apparent resistivity has been measured by Schlumberger profiling, and the data transmitted to a PC for interpretation. Various layers' apparent resistivity was converted to their absolute resistivity. Using the IP2Win software, the resistivity with thickness and depth of each stratum was also determined.

VES method (also known as resistivity depth proving) is used whenever the depth section of a particular place is required. VES offers information about change in the lithology with depth by means of measured resistivity at surface. Two pairs of electrodes are needed for VES measurements: electrodes M and N are used for current injections, while electrodes A and B are for potential difference measurements (Figure 4). The current electrodes are shifted for each measurement, leaving the potential electrodes in place. The potential electrodes are moved only when the signal becomes too weak to be measured [29]. VES method quantifies the potential field generated by current flowing into the subsurface where contiguous contrast of electrical resistivity is measured [16]. This approach measures the depth of influence below the sub-surface in direct proportion to the distance between the current electrodes at a fixed center. The greater distance between current electrodes permits greater current penetration beneath the subsurface, allowing for the extraction of properties such as depth, thickness, and resistivities. In general, for sub-surface formations, four electrodes are used for measuring the resistivities. Depending on the purpose of sub-surface exploration, different electrode arrangements can be made to measure the potential difference. Although VES method works with both Wenner and Schlumberger configurations, Schlumberger has a little advantage. The Schlumberger approach is simple to use but challenging to understand [53].

Present study considers one dimensional geo-electrical survey, i.e. VES for groundwater exploration. VES method of geophysics prospecting that widely used to image the shallow subsurface for groundwater exploration [54]. At the investigation point, the variations in the subsurface electrical resistivity in vertical direction are measured. Modelling the sub-surface as a series of horizontally stacked layers with only depth-dependent changes in resistivity. Thus the model of interpretation of VES is one dimensional (1D) and inherently insensitive to lateral variations in sub-surface resistivity, which can result in substantial changes in apparent resistivity values [55]. According to the layout of the Schlumberger arrays, the distance between the current electrodes (M and N) is at least five times greater than that between the potential electrodes (A and B) (Figure 4). The most common arrays are Schlumberger, Wenner. The arrays differ each other in terms of depth of investigation, vertical and horizontal resolution, and signal strength [56]. In the vertical electrical sounding (VES) method of groundwater research, the Schlumberger array is frequently employed. The Schlumberger array has the benefits of having a small cable require for the potential electrodes and requiring fewer electrodes to be moved for each sounding. Schlumberger soundings generally have better resolution, greater probing depth, and less time-consuming field deployment than the Wenner array [57]. Hence, each array has its own distinct benefits and draw backs. The selection of an appropriate array is stated to be influenced by the material's depth, the type of heterogeneity to be mapped, the presence or absence of vertical and horizontal shifts in the subsurface, and the strength of the signal. However, the primary thing to examine is the survey's purpose. The study of Samouëlian *et al.* [58] emphasizes that in certain instances, the employment of diverse configurations might

improve the varied reading properties of the subsoil, leading to a more accurate interpretation. From the previous discussion, it is concluded that the Schlumberger configuration is characterized with best vertical resolution, greater probing depth, more sensitivity to the vertical variation of resistivity and is less time-consuming than other arrays [56]. Therefore, the Schlumberger array (Figure 4) has been employed in the present study.

A total of 40 VES measurements were obtained within the studied area using the Schlumberger electrode design. The conventional partial curve technique and auxiliary point diagrams combined with two-layer master curves accomplish the preliminary VES data [59]. The software IPI2WIN is utilized for computer-aided interpretation in which initial parameters such as the layer resistivity and thickness are determined [60]. The longitudinal conductance (S) is considered the significant geophysical parameter for n layers and given by Equation (1) (Zohdy *et al.* [61]:

$$S = \sum_{i=1}^{n} (hi/\rho i) \quad (1)$$

where hi and ρi represent the saturated thickness of each layer and true resistivity, respectively.

Relatively overburden of thick succession is represented by a higher value of S, which is allotted a higher priority to evaluate the groundwater potential. The protected aquifer's capacity is likewise determined using these values. Both the parameters i.e. longitudinal conductance (S) and the protective capacity are well-correlated. If any change in the value of longitudinal conductance affect the protective capacity. Therefore, the values of total longitudinal conductance (S) were used to calculate the aquifer's protective capacity over the research area.

Figure 3. Resistivity meter (Model: SSR–MP–AT).

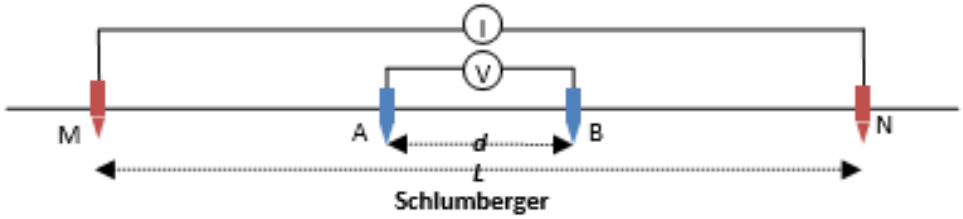

Figure 4. Schlumberger array configuration.

2.3. Preparation of spatial distribution maps

The ArcGIS 10.1 software has performed the spatial pattern analysis for the various sub-surface layer parameters including aquifer resistivity (AR), layer thickness (LT), longitudinal conductance (S), and transverse resistivity (TR). Figures 5-8 show the maps of these subsurface layer parameters i.e. AR, LT, S, and TR, respectively. These sub-surface layer parameters are presented for 2nd, 3rd, 4th, and 5th sub-surface stratum. The water table is certainly below the first layer, which always unsaturated. The inverse distance weighted (IDW) interpolation tool and the spatial analyst tool in ArcGIS were used to determine the spatial distribution of aquifer characteristics such as aquifer thickness, aquifer resistivity (AR), transverse resistance (TR), and longitudinal conductance (S) [62]. Such an approach has been utilized by many researchers [63-66]. The IDW data was classified into five

categories for the second, third, and forth layers and three categories for the fifth layer using defined interval. The interval size and the largest sample size using a set interval determine the number of categories. The interval size must be as narrow as possible to accommodate the three categories that are the minimum allowed. Therefore, three categories of IDW data are found appropriate for fifth layer and five categories for the second, third, and fourth layers.

Another analysis for aquifer thickness was calculated using the ArcGIS spline interpolation method. The spline tool uses an interpolation technique that establishes value using a mathematical function that reduces surface curvature overall. Splines' use is simpler and more natural because of its physical interpretation.

3. Results and Discussion

The following indices were used to measure the groundwater potential of the region: aquifer resistivity (AR), longitudinal conductance (S), layer thickness (LT), and transverse resistivity (TR). Table 2 shows the interpreted geo-electric parameters, i.e. the studied area's AR, LT, and mean S. A second sub-surface layer was observed, with 66.63% of its area attributable to this layer. On the other hand, the maximum layer thickness of the third subsurface geo-electric layer is observed as 180.00 m. The average thickness of 46.65 m, 25.05 m, 8.74 m, and 11.62 m were recorded for layers 2, 3, 4, and 5, respectively. It was also observed that the second layer has a higher aquifer protection capacity (APC) against aquifer pollution due to its higher average longitudinal conductivity (S) compared to the other three layers [67, 69]. From layers 2 to 5, a declining trend in TR values was observed, indicating reduced aquifer potential in deeper strata. The transverse resistance maps for different sublayers (Figure 8) and the value vary for most protective layer from 143.75 Ω-m^2 to 29443.68 Ω-m^2 (Figure 8p). The eastern zone of the study region contains the highest TR value. The zone where the protective layer's thickness and resistivity are highest corresponds to the maximum value of TR.

Table 1. Well depth and water table information (Singh and Tripura [50]).

Latitude	Longitude	Water table (m) (Bgl)	Well depth (m)	Source type
31.707	76.523	18.00	60	Borehole
31.709	76.526	12.00	50	-
31.702	76.524	39.00	65	-
31.704	76.524	25.00	70	-
31.704	76.525	60.00	70	-
31.704	76.525	72.00	150	-
31.707	76.529	81.00	150	-
31.706	76.527	90.00	150	-
31.675	76.533	98.00	120	-
31.676	76.534	102.00	120	-
31.884	76.584	2.73	80	-
31.872	76.641	1.67	40	-
31.494	76.497	4.13	82	-
31.624	76.707	9.60	84	-
31.759	76.367	5.32	82	-
31.735	76.352	5.16	61	-

Note: Bgl refers to measurement of water table is below the ground level at the concerned site.

Table 2. Table displaying the stratified layers acquired with VES at various points.

VES Nos	Resistivity (Ω-m)					Thickness (m)					ρ_a	S
	ρ_1	ρ_2	ρ_3	ρ_4	ρ5	h1	h2	h3	h4	h5		
VES 2	36.5	42.0	220.0	-	-	2.5	94.49	6.0	-	-	42.0	2.25
VES 37	225	45.0	225.3	-	-	3.5	54.86	5.0	-	-	45.0	1.22
VES 27	613.5	39.0	213.0	-	-	45.0	65.06	11.0	-	-	39.0	1.67
VES 28	650	56.0	316.0	-	-	6.5	45.72	21.3	-	-	56.0	0.82
VES 38	112.5	70.0	325.5	-	-	11.1	51.82	8.0	-	-	70.0	0.74
VES 39	98.5	163.0	354.3	-	-	5.5	109.73	9.0	-	-	163.0	0.67
VES 18	236	94.3	13.1	-	-	46.00	58.10	45.79	-	-	236.0	0.20
VES 19	125	28.9	1.06	-	-	26.0	44.0	10.0	-	-	125.0	0.97
VES 26	326.0	12.5	-	-	-	7.79	85.3	-	-	-	326.0	0.99
VES 5	13.6	60.0	-	-	-	45.0	57.91	-	-	-	60.0	0.79
VES 6	10.0	68.0	-	-	-	30.0	67.06	-	-	-	68.0	0.80
VES 7	158	100.0	-	-	-	15.5	79.25	-	-	-	100.0	0.28
VES 4	14.3	95.0	-	-	-	10.0	76.20	-	-	-	95.0	0.15
VES 20	39.5	322.0	-	-	-	4.5	91.44	-	-	-	322.0	0.32
VES 8	12.3	350.0	-	-	-	12.5	51.82	-	-	-	350.0	0.24
VES 29	18.2	254.3	250.0	-	-	2.0	13.0	79.25	-	-	250.0	0.28
VES 9	18.5	124.5	325.0	-	-	3.5	10.0	79.25	-	-	325.0	1.35
VES 1	25.3	100.2	125.0	-	-	11.6	2.0	34.87	-	-	125.0	2.88
VES 25	28.3	100.9	198.0	306.2	-	12.5	4.0	10.61	15.5	-	198.0	0.30
VES 21	26.5	214.3	355.0	-	-	13.6	45.0	4.65	-	-	355.0	0.14
VES24	33.2	95.5	260.0	60.5	-	12.2	4.0	4.81	12.5	-	260.0	1.36
VES 3	38.2	96.3	58.5	658.7	-	13.5	3.0	79.25	10.0	-	58.5	1.15
VES 30	43.2	125.5	62.5	-	--	15.5	4.0	180.0	-	-	62.5	0.15
VES 16	56.3	126.5	158.0	313.0	125	5.0	24.0	16.44	6.5	10.5	158.0	0.01
VES 23	10.8	12.5	325.0	122.3	94.5	4.0	25.0	97.54	5.2	10	325.0	8.88
VES 15	44.8	121.2	102.0	125.4	99.4	48.33	10.0	13.98	5.0	12.5	102.0	0.11
VES 31	15.4	11.5	32.5	124.0	90.8	12.9	12.5	44.20	6.5	13.5	32.5	0.37
VES 22	60.1	436.0	12.3	-	-	2.36	14.32	14.32	-	-	436.0	4.35
VES 32	22.2	45.0	224.3	-	-	3.5	51.82	6.5	-	-	45.0	2.20
VES 14	19.5	325.0	125.5	-	-	6.5	48.77	3.5	-	-	325.0	0.18
VES 33	26.4	125.0	99.2	-	-	2.5	10.41	2.5	-	-	125.0	2.25
VES 34	32.5	355.0	90.9	-	-	2.5	2.90	10.0	-	-	355.0	1.22
VES 36	33.5	10.3	244.5	-	-	10.5	91.44	2.5	-	-	10.3	1.67
VES 17	31.3	12.5	95.5	-	-	9.5	68.08	2.5	-	-	12.5	0.82
VES 40	28.9	375.0	96.4	-	-	10.0	42.67	5.5	-	-	375.0	0.74
VES 35	44.5	125.0	122.5	-	-	6.5	45.72	5.0	-	-	125.0	0.67
VES 10	62.5	38.0	128.6	-	-	2.5	164.66	4.0	-	-	38.0	0.20
VES 11	12.8	10.5	10.5	-	-	3.5	45.72	3.0	-	-	10.5	0.97
VES 12	15.8	18.0	214.3	-	-	4.5	39.62	3.0	-	-	18.0	0.99
VES 13	18.4	285.0	112.5	-	-	4.0	50.79	3.5	-	-	285.0	0.79

3.1. Spatial distribution maps showing layer thickness and layer resistivity

The thickness map of the subsurface layers is shown in Figure 6. Layer 2 thickness ranges from 2 to 164.66 m (Figure 6p), Layer 3 from 2.5 to 18.0 m (Figure 6q), Layer 4 from 5 to 15.5 m (Figure 6r), and Layer 5 from 10 to 13.5 m (Figure 6s). The second sub-surface geo-electric layer indicates the greater part of the area (66.63%). The maximum thickness for the second layer can be seen in the western region of the studied area (Figure 6p). The largest area of thick overburden is expected to produce an economically usable amount of groundwater [69]. The extremely thin protective sublayer may not be prevalent, so the sitting of boreholes in such areas is discouraged [70]. In the

research area, the aquifer is considered to be the most productive stratum. Figure 12 displays a map of the research area's aquifer thickness. Using the ArcGIS software, spline interpolation was used to display the aquifer thickness map for the current investigation. Spline tool employs an interpolation methodology that determines value with a mathematical function which minimizes overall surface curvature. The physical interpretation of splines makes their application easier and more intuitive. Sujanpur, Bhoranj, and Barsar are the three administrative units in the studied area with aquifer thickness values that are substantially lower than the average value, while Nadaun and Hamirpur have aquifer thickness value that is particularly higher than the average value. Barsar has the thickest aquifer (180.08 m), followed by Nadaun (164.66 m), Hamirpur (109.72 m), Bhoranj (97.53 m), and Sujanpur (91.43 m).

Values of resistivity contrast can reveal information about a location's potential for groundwater. Figure 5 shows the spatial distribution of AR value for different layers. VES 4-8, VES 20, and VES 26 represent the minimal layer types. Simultaneously, VES 15, VES 16, VES 23, and VES 31 contain the maximum number of layer types. The lowest resistivity value is 1.06 ohm-m for the third layer of VES 19 (Fig 5r). The fourth layer of VES 3 indicates a maximal resistivity value of 658.7 ohm-m (Figure 5s). Figure 11 depicts the interpretation of resistivity values for the earth materials and lithologies of the borehole record. The lithology of VES 22 is described as sandstone, conglomerate, and clay based on interpretations of the sounding curve. Sandstone is the predominant aquifer stratum in this region. In this type of layer high resistivity value i.e. 436 Ohm-m are recorded.

3.2. Transverse resistance

Transverse resistance (TR) called as geo-electrical parameter and plays important role for qualitative analysis of the aquifer system. Transverse resistance (TR), also known as the Dar-Zarrouk parameter, is a secondary geoelectrical parameter that is crucial for developing a qualitative assessment of the aquifer system [61]. It is directly related to transmissivity; the zone of the aquifers with high transmissivity is affected by the greatest TR values, and vice versa [71, 72]. According to Nwachukwu *et al*. [73], one of the geoelectric characteristics used to define the area of groundwater potential is called TR.

It is so named because of their dependence on fundamental characteristics like resistivity (ρ) and layer thickness (h), they are given this name. Mathematically, the transverse resistance of any geological formation is correlated with the resistivity (ρ) (Ω-m) and aquifer thickness (h) (m) and defined by the equation (2).

$$TR = \rho_i \times h_i \quad \{i = 1,2,3,\ldots \text{nth layers}\} \quad (2)$$

The measurement of transverse resistance aids in identifying prospective groundwater quality.

The spatial distribution maps for different sub-layers, i.e. second, third, fourth, and fifth have been prepared. From layer second to fifth, a declining trend in TR values was observed, indicating reduced aquifer potential in deeper strata. The transverse resistance maps of different sublayers are shown in the Figures 8p-8s. The transverse resistance value ranges from 143.75 Ω-m^2 to 29443.68 Ω-m^2 for most protective layer (Figure 8p). The maximum value of TR is recorded in the eastern zone of the studied area. The region where the protective layer's thickness and resistivity are highest corresponds to the maximum value of TR.

3.3. Longitudinal conductance (S) and aquifer protective capacity

The thicknesses and layer resistivities were interpreted and utilized to calculate the longitudinal conductance. S-values were determined for the underlying aquifer's ability to protect itself against encroaching contaminants. S-values help assess the protective capacity of an aquifer [68, 74]. To determine the potability of the water and the aquifer's sensitivity to contamination, it is crucial to evaluate the area's aquifer protective capacity. The higher S value of an area is used to interpret the higher protective capacity of an aquifer [75]. Conversely, reduced aquifer transmissivity is a sign of the increase in S value [76]. The longitudinal conductance is determined using Equation 1. Figures 7 and 9 show the spatial distribution of S values for geoelectrical subsurface layers and aquifers in the study area. The aquifer in the studied area has longitudinal conductance values that range from 0.01 to 8.88 mhos. The protective capacity rating based on the S values (in mhos) [68, 71] is as follows; S - < 0.1 (poor), 0.1 to 0.19 (weak), 0.2 to 0.69 (moderate), 0.7 to 4.9 (good), 5 to 10 (very good), and > 10 (excellent). The protective capacity rating as per Oladapo *et al*. [63]; Oladapo and Akintorinwa [74] is found suitable for the present study which is confirmed with the field data of CGWB [52].

There is variation in the S values for different sublayers, as seen in Figures 7p-7s. Materials possessed a weak and poor protective capacity rating for the fifth layer, where the maximum value is 0.15 (Figure 7s). Table 3 provides an overview of the research area's aquifer protective capacity rating. Figure 8 displays the dispersion of zones for various categories in terms of protective capacity. The weaker and poorer areas are more vulnerable to pollution. The S values indicate that the area can be classified into five categories, i.e., Poor (5.55%), weak (19.43%), moderate (19.45%), good (38.89%), and very good (16.68%). However, it can be seen that most areas are under the good category. It is possible to attribute topography and geological structure to the variance in sub-surface layer thickness in this area (Figure 6).

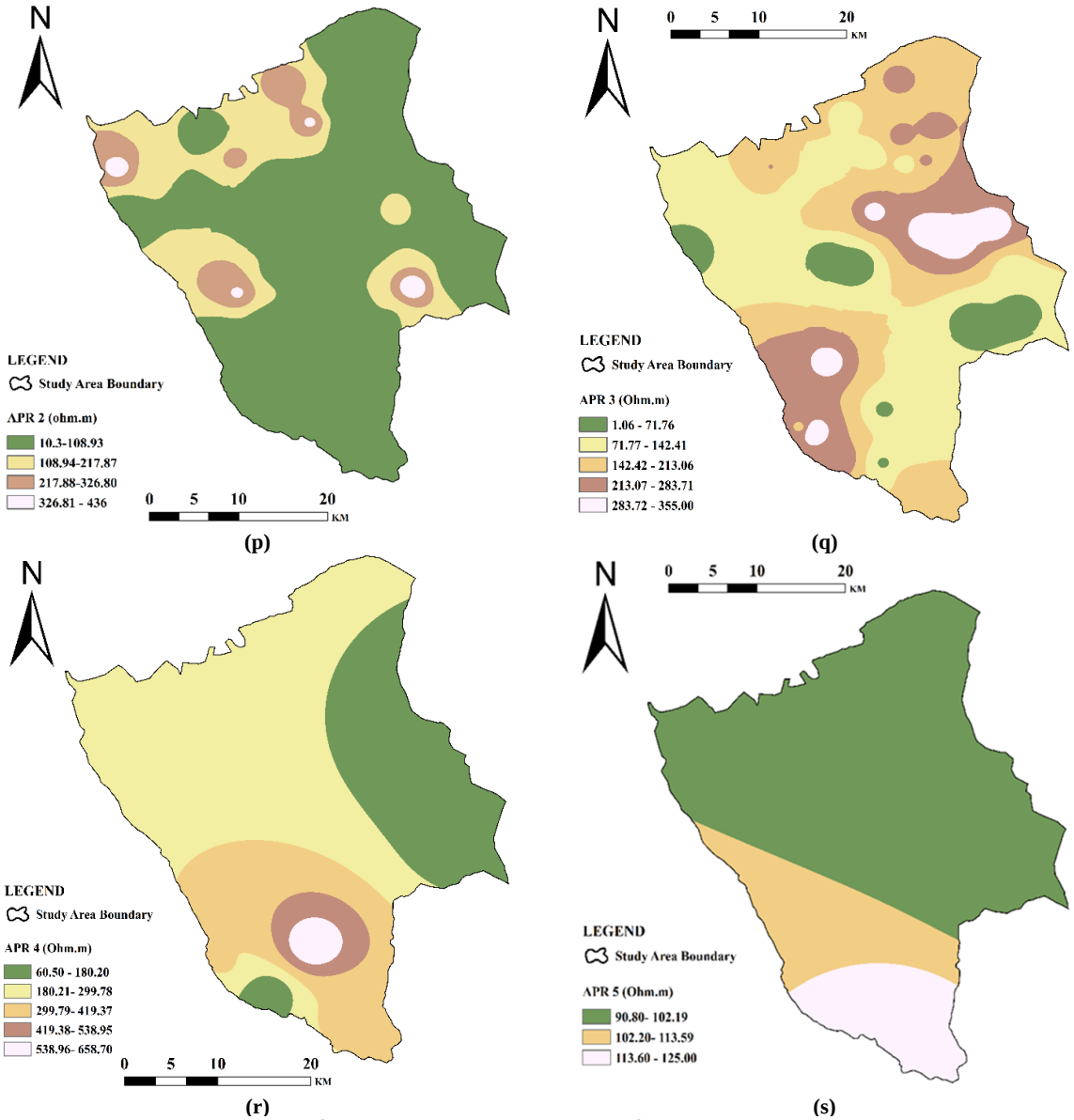

Figure 5. p) AR value map for 2nd strata, q) AR value map for 3rd strata, r) AR value map for 4th strata, s) AR value map for 5th strata.

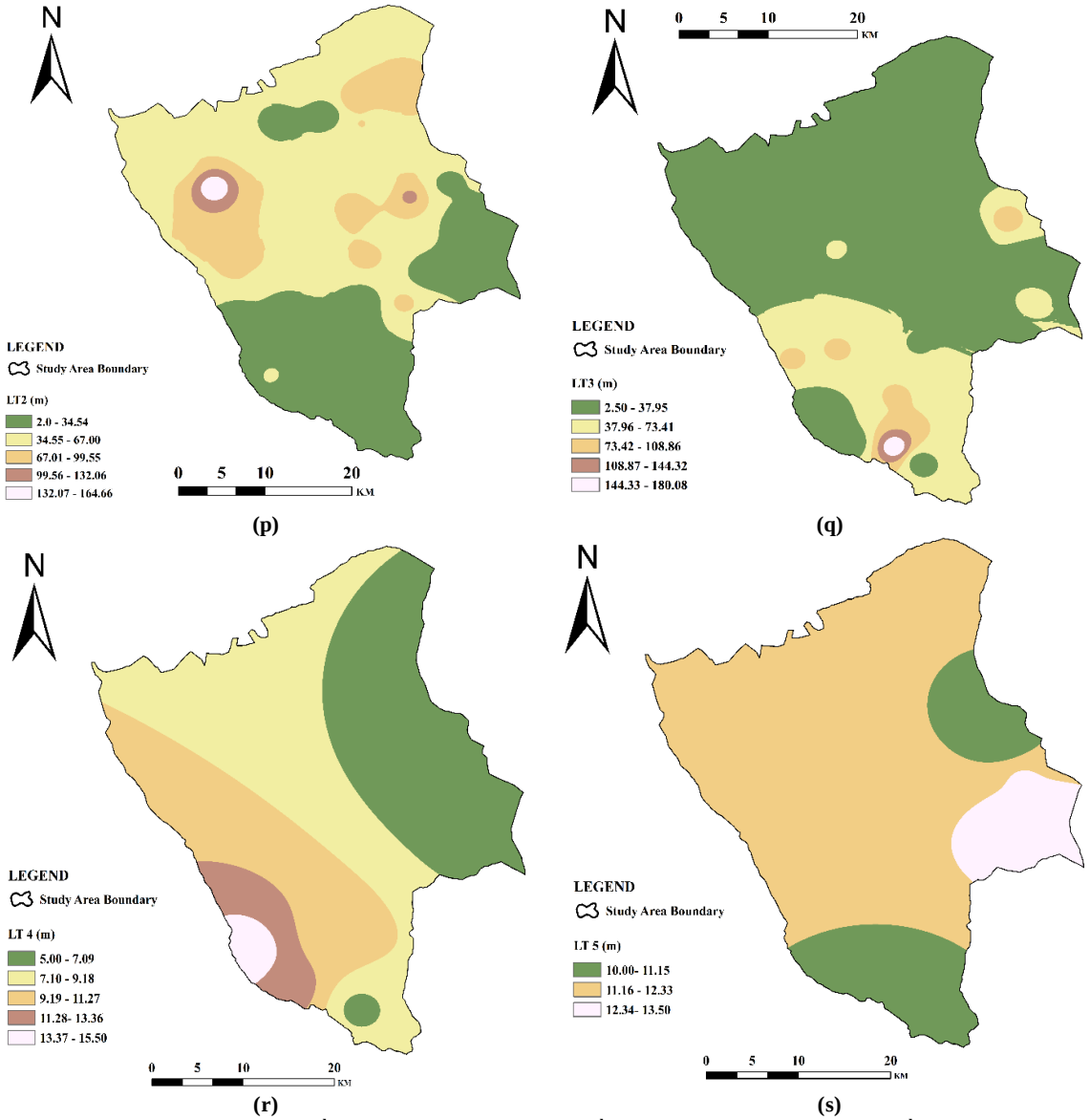

Figure 6. p) LT value map for 2nd strata q) LT value map 3rd strata, r) LT value map for 4th strata, s) LT value map for 5th strata.

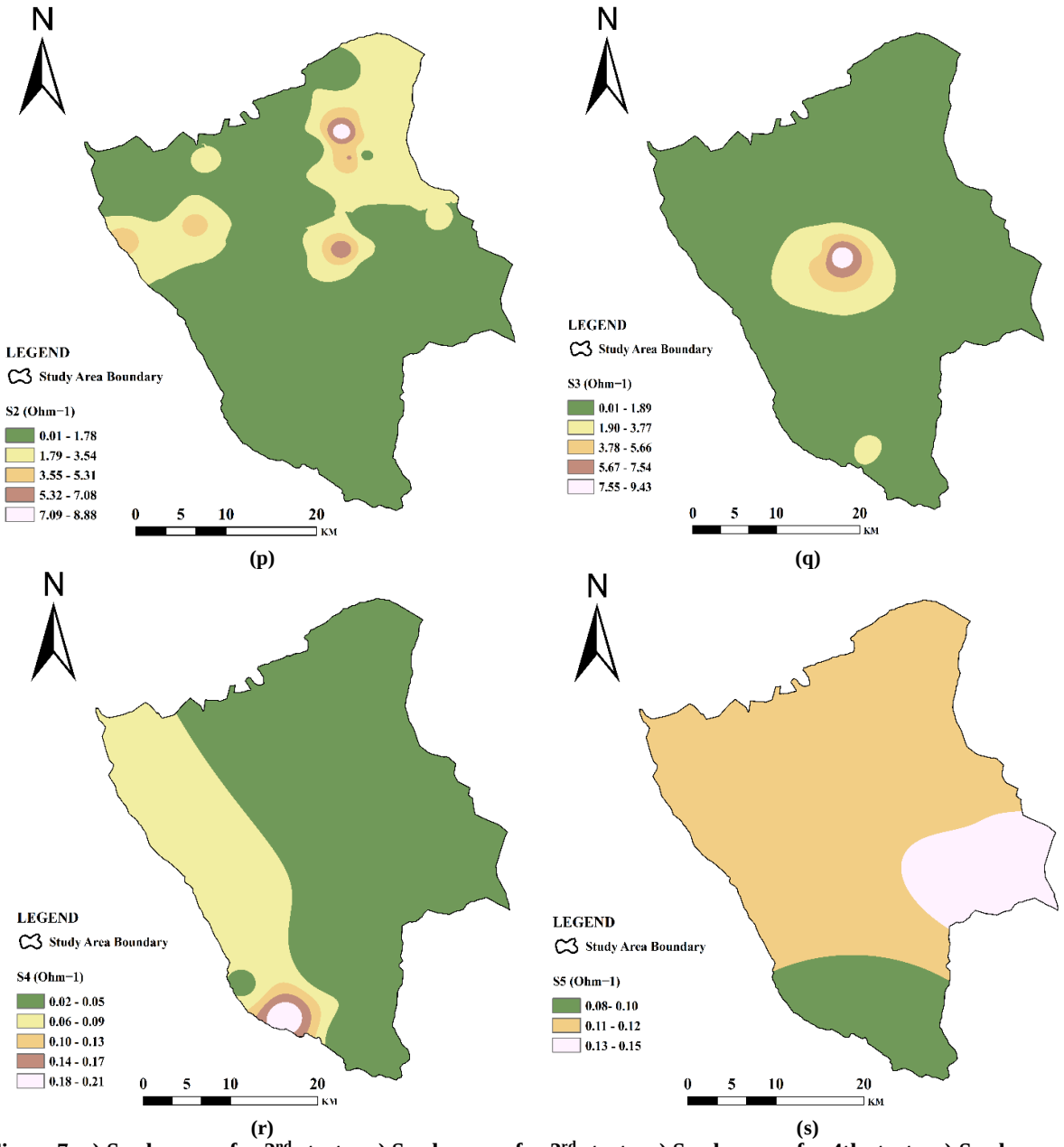

Figure 7. p) S value map for 2nd strata, q) S value map for 3rd strata, r) S value map for 4th strata, s) S value map for 5th strata.

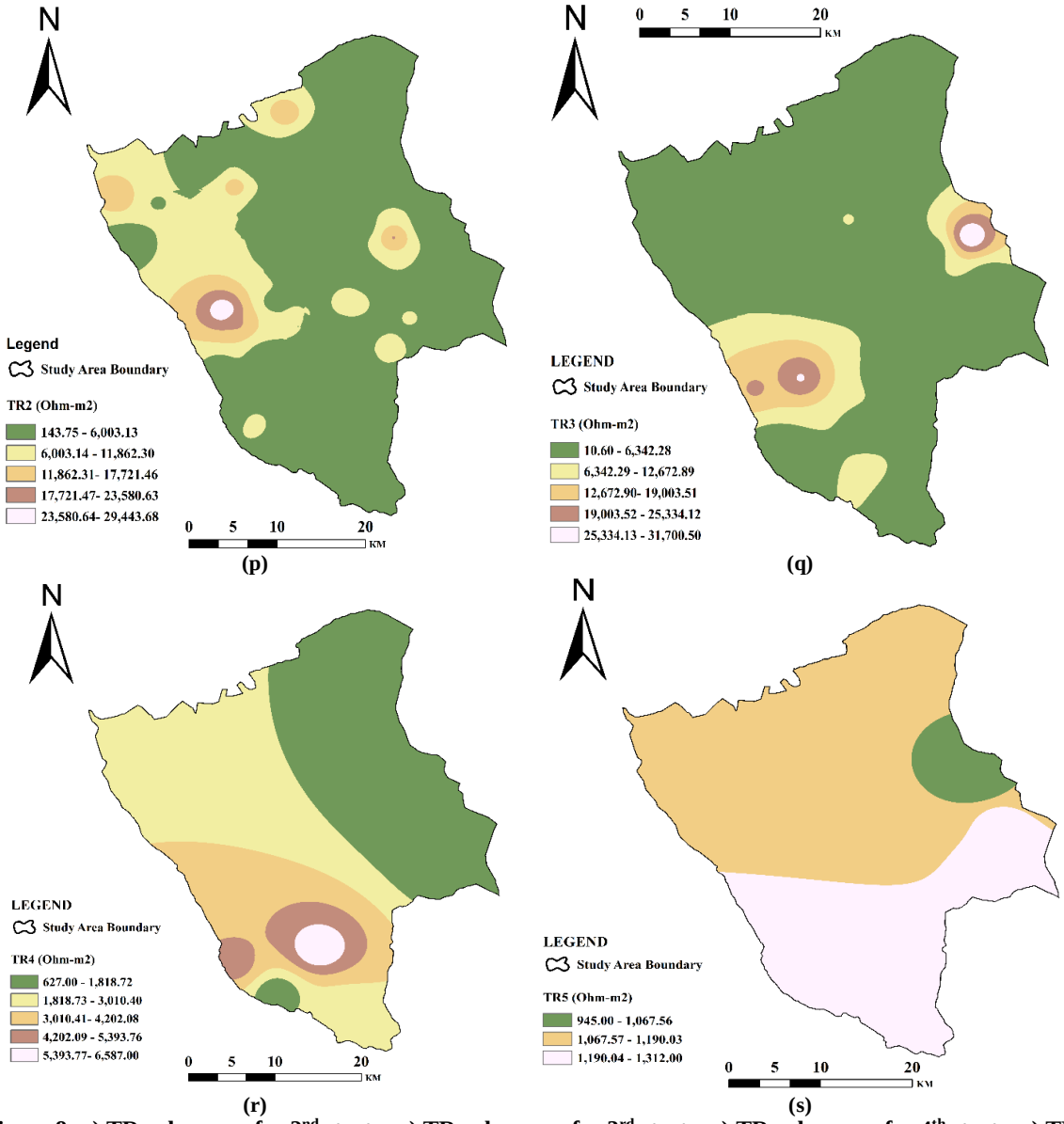

Figure 8. p) TR value map for 2nd strata, q) TR value map for 3rd strata, r) TR value map for 4th strata, s) TR value map for 5th strata.

The spatial pattern analysis for the different sub-surface layer parameters such as aquifer resistivity (AR), layer thickness (LT), longitudinal conductance (S), and transverse resistivity (TR) has done in the ArcGIS 10.1 software, and shown in Figures 5-8.

Table 3. Protective capacity rating of aquifers (after Oladapo *et al*. [68] and Oladapo & Akintorinwa [74])

Rating category	VES location
Very Good	VES17, VES36
Good	VES2, VES3, VES4, VES5, VES6, VES7, VES10, VES11, VES12, VES27, VES28, VES30, VES31, VES32, VES37, VES38
Moderate	VES1, VES9, VES18, VES19, VES20, VES23, VES29, VES35, VES39
Weak	VES8, VES14, VES15, VES16, VES40
Poor	VES13, VES21, VES22, VES24, VES25, VES26, VES33, VES34

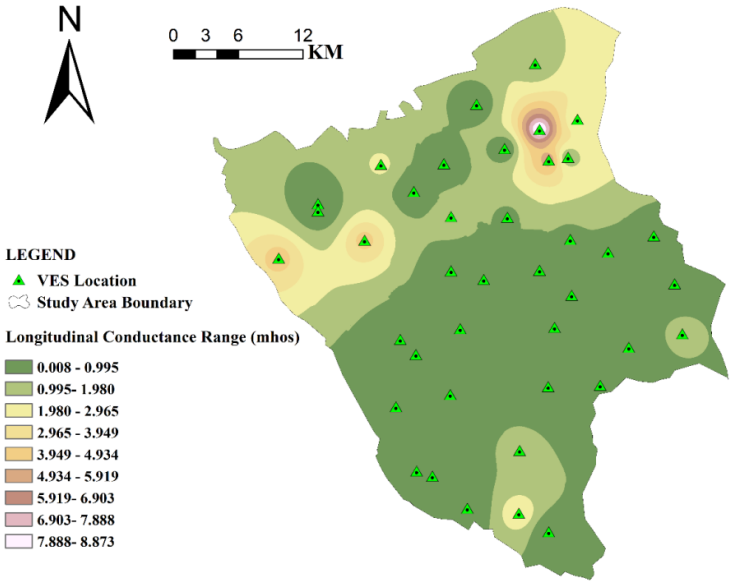

Figure 9. Longitudinal conductance value map of the aquifer.

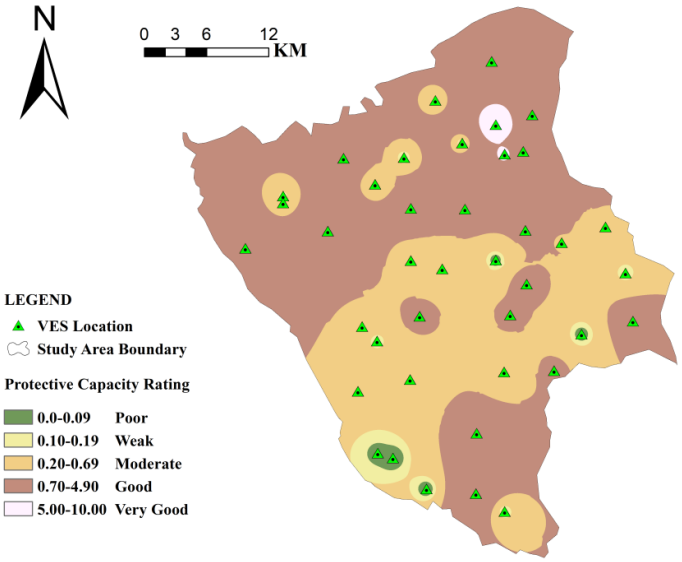

Figure 10. Protective capacity map of the studied area.

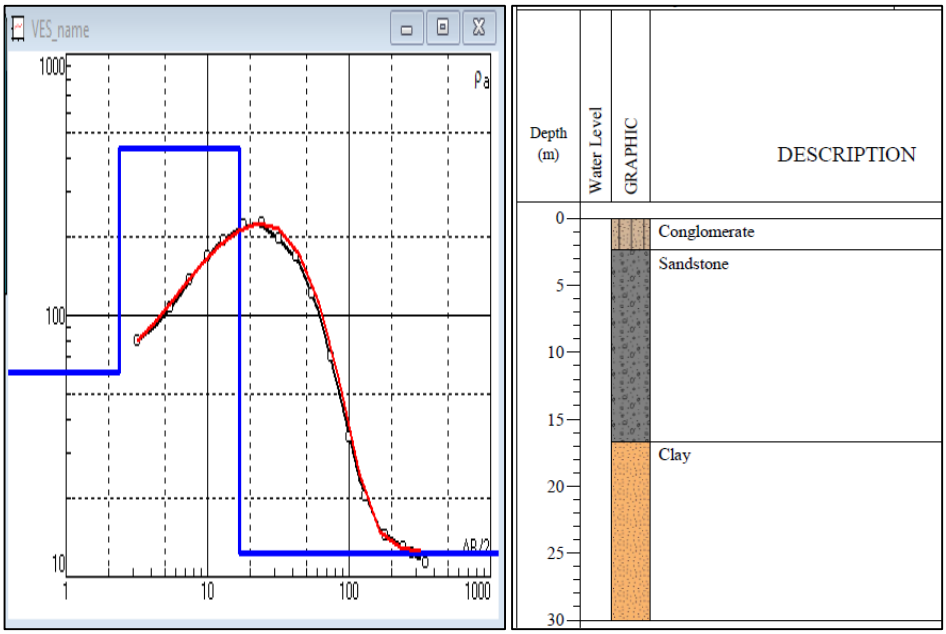

Figure 11. VES 22 is close to the bore-well and lithology.

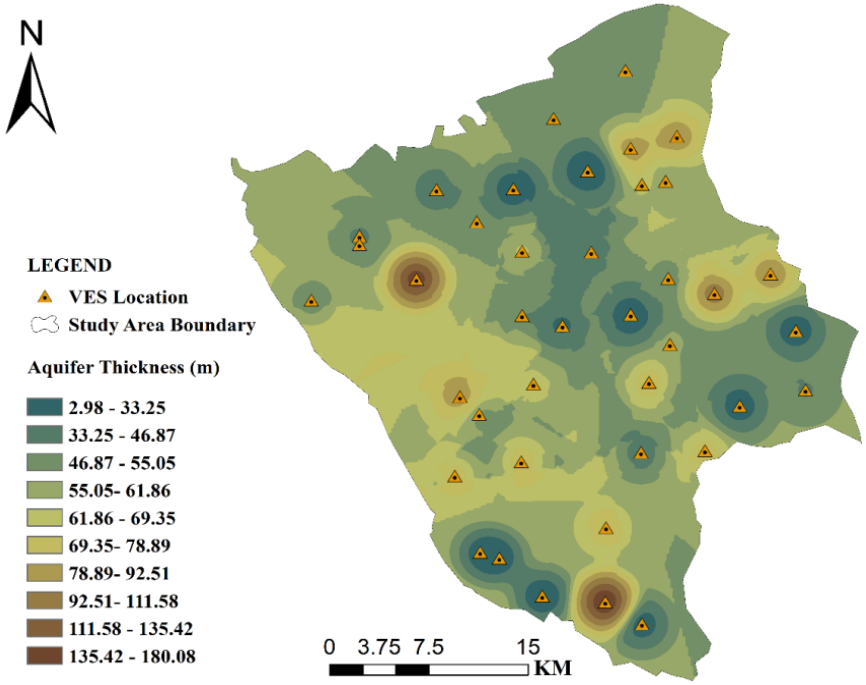

Figure 12. Aquifer thickness map.

4. Conclusions

A VES survey has been carried out to identify possible groundwater zones and determine the capacity of the protective/covering layers of the underlying aquifer repository. The results of the survey were used to prescribe effective aquifer depth for the Hamirpur district of H.P. (India) groundwater budget. The aquifer present in the study area is confined in nature. The topsoil is efficient based on the S values for protecting the underlying aquifer. The longitudinal conductance (S), which is an important indicator of aquifer health in terms of protective capacity has been estimated based on aquifer thickness and resistivity. The aquifer potential is classified on the basis of S values as poor for less than 0.1 mhos, weak for the range of 0.1-0.19 mhos, moderate for the range of 0.2-0.69 mhos, good for the range of

07-0.49 mhos, very good for the range of 5-10 mhos and excellent for greater than 10 mhos. The obtained values of S indicate that 65% of the study area falls under moderate conditions. This means that the aquifer is protected from contaminant intrusion. S results demonstrate that two VES locations are within the *very good* category zones, 16 VES under the *good* category, nine under the *moderate* category, five under the *weak* category, and eight under the *poor* category. Five geoelectric layers were identified, i.e. topsoil, fractured sandstone/gravel/sand, clay mix gravel/clay mix sand/ coarse-grained sandstones, conglomerate/clay/hard sandstone, and sandstone/shale. Based on data interpretation and analysis, the study postulates that the second and third sub-layer are characterized to yield more water in the research area, which confirms the study area's geology. The research work demonstrates the effectiveness of the methods used to quickly gather additional data for the evaluation of aquifer parameters, sub-surface lithology examination, classification of aquifer types, evaluation of a region's protective capacities, groundwater potential, and potential well locations. The present study may further be supported by using other suitable approaches such as test drilling, borehole sensing, etc. for positioning bore well settings and in prospecting potential groundwater zones especially in hilly terrain regions for better outcomes.

Acknowledgments

The authors would like to thank the Central Ground Water Board (CGWB), North Himalayan Region (NHR), Dharamsala, Himachal Pradesh, for providing the data. We also thank the National Institute of Technology, Hamirpur's Department of Civil Engineering for providing research facilities.

References

[1]. Grönwall, J., & Danert, K. (2020). Regarding groundwater and drinking water access through a human rights lens: Self-supply as a norm. *Water*, *12*(2), 419.

[2]. Giordano, M., & Villholth, K. G. (Eds.). (2007). *The agricultural groundwater revolution: opportunities and threats to development* (Vol. 3). CABI.

[3]. Qureshi, A. S. (2015). Improving food security and livelihood resilience through groundwater management in Pakistan. *Glob. Adv. Res. J. Agric. Sci*, *4*, 687-710.

[4]. Dangar, S., Asoka, A., & Mishra, V. (2021). Causes and implications of groundwater depletion in India: A review. *Journal of Hydrology*, *596*, 126103.

[5]. Walker, D. W., Cavalcante, L., Kchouk, S., Ribeiro Neto, G. G., Dewulf, A., Gondim, R. S., Martins, E. S. P. R., Melsen, L. A., de Souza Filho, F. D. A., Vergopolan, N., & Van Oel, P. R., (2022). Drought diagnosis: What the medical sciences can teach us. *Earth's Future*, *10*(4), e2021EF002456.

[6]. Wada, Y., & Bierkens, M. F. (2014). Sustainability of global water use: past reconstruction and future projections. *Environmental Research Letters*, *9*(10), 104003.

[7]. Konikow, L. F. (2015). Long-term groundwater depletion in the United States. *Groundwater*, *53*(1), 2-9.

[8]. Elbeltagi, A., Salam, R., Pal, S. C., Zerouali, B., Shahid, S., Mallick, J., Islam, M.S., & Islam, A. R. M. T. (2022). Groundwater level estimation in northern region of Bangladesh using hybrid locally weighted linear regression and Gaussian process regression modeling. *Theoretical and Applied Climatology*, *149*(1-2), 131-151.

[9]. Carter, R., Chilton, J., Danert, K., & Olschewski, A. (2014). Siting of drilled water wells—a guide for project managers, rural water supply network (RWSN), St Gallen, Switzerland.

[10]. Adimalla, N., Li, P., & Venkatayogi, S. (2018). Hydrogeochemical evaluation of groundwater quality for drinking and irrigation purposes and integrated interpretation with water quality index studies. *Environmental Processes*, *5*, 363-383.

[11]. Maity, S., Biswas, R., & Sarkar, A. (2020). Comparative valuation of groundwater quality parameters in Bhojpur, Bihar for arsenic risk assessment. *Chemosphere*, *259*, 127398.

[12]. Banerjee, S., & Sikdar, P. K. (2022). Hydrochemical fingerprinting and effects of urbanisation on the water quality dynamics of the Quaternary aquifer of south Bengal Basin, India. *Environmental Earth Sciences*, *81*(4), 134.

[13]. Kenneth, S. O., & Edirin, A. (2012). Determination of aquifer properties and groundwater vulnerability mapping using geoelectric method in Yenagoa City and its environs in Bayelsa State, South South Nigeria. *Journal of Water Resource and Protection*, 2012.

[14]. Bello, H. I., Alhassan, U. D., Salako, K. A., Rafiu, A. A., Adetona, A. A., & Shehu, J. (2019). Geoelectrical investigation of groundwater potential, at Nigerian Union of Teachers Housing estate, Paggo, Minna, Nigeria. *Applied Water Science*, *9*, 1-12.

[15]. Kalinski, R. J., Kelly, W. E., & Bogardi, I. (1993). Combined use of geoelectric sounding and profiling to quantify aquifer protection properties. *Groundwater*, *31*(4), 538-544.

[16]. Bery, A. A., Saad, R., Mohamad, E. T., Jinmin, M., Azwin, I. N., Tan, N. A., & Nordiana, M. M. (2012). Electrical resistivity and induced polarization data correlation with conductivity for iron ore exploration.

The Electronic Journal of Geotechnical Engineering, *17*, 3223-3233.

[17]. Kepic, A., & Javadipour, S. (2015). Resistivity and Induction polarization technique for mapping hematite rich areas in Iran. *ASEG Extended Abstracts*, *2015*(1), 1-4.

[18]. Shin, Y., Shin, S., Cho, S. J., & Son, J. S. (2021). Application of 3D Electrical Resistivity Tomography in the Yeoncheon Titanomagnetite Deposit, South Korea. *Minerals*, *11*(6), 563.

[19]. Hinojosa, H. R., Kirmizakis, P., & Soupios, P. (2022). Historic underground silver mine workings detection using 2D electrical resistivity imaging (Durango, Mexico). *Minerals*, *12*(4), 491.

[20]. Olenchenko, V. V., Bortnikova, S. B., & Devyatova, A.Yu. (2023). Application of electrical prospecting methods for technogenic bodies (stored wastes of the mining industry) studies: a review. *Russian Journal of Geophysical Technologies*, *4*, 23-40.

[21]. Dimech, A., Cheng, L., Chouteau, M., Chambers, J., Uhlemann, S., Wilkinson, P., Meldrum, P., Mary, B., Fabien-Ouellet, G., & Isabelle, A. (2022). A review on applications of time-lapse electrical resistivity tomography over the last 30 years: perspectives for mining waste monitoring. *Surveys in Geophysics*, *43*(6), 1699-1759.

[22]. Shokri, B. J., Ramazi, H., Ardejani, F. D., & Moradzadeh, A. (2014). Integrated time-lapse geoelectrical-geochemical investigation at a reactive coal washing waste pile in Northeastern Iran. *Mine Water and the Environment*, *33*(3), 256.

[23]. Shafaei, F., Ramazi, H., Shokri, B. J., & Ardejani, F. D. (2016). Detecting the source of contaminant zones down-gradient of the alborz Sharghi coal washing plant using geo-electrical methods, northeastern Iran. *Mine Water and the Environment*, *35*(3), 381.

[24]. Jodeiri Shokri, B., Doulati Ardejani, F., & Moradzadeh, A. (2016). Mapping the flow pathways and contaminants transportation around a coal washing plant using the VLF-EM, Geo-electrical and IP techniques—A case study, NE Iran. *Environmental Earth Sciences*, *75*, 1-13.

[25]. Shokri, B. J., Ardejani, F. D., Ramazi, H., & Moradzadeh, A. (2016). Predicting pyrite oxidation and multi-component reactive transport processes from an abandoned coal waste pile by comparing 2D numerical modeling and 3D geo-electrical inversion. *International Journal of Coal Geology*, *164*, 13-24.

[26]. Jodeiri Shokri, B., Shafaei, F., Doulati Ardejani, F., Mirzaghorbanali, A., & Entezam, S. (2023). Use of time-lapse 2D and 3D geoelectrical inverse models for monitoring acid mine drainage-a case study. *Soil and Sediment Contamination: An International Journal*, *32*(4), 376-399.

[27]. Arjwech, R., & Everett, M. E. (2015). Application of 2D electrical resistivity tomography to engineering projects: Three case studies. *Songklanakarin Journal of Science & Technology*, *37*(6).

[28]. Amini, A., & Ramazi, H. (2016). Application of electrical resistivity imaging for engineering site investigation. A case study on prospective hospital site, Varamin, Iran. *Acta Geophysica*, *64*, 2200-2213.

[29]. Akingboye, A. S., & Osazuwa, I. B. (2021). Subsurface geological, hydrogeophysical and engineering characterization of Etioro-Akoko, southwestern Nigeria, using electrical resistivity tomography. *NRIAG Journal of Astronomy and Geophysics*, *10*(1), 43-57.

[30]. Kumar, D., Thiagarajan, S., & Rai, S. N. (2011). Deciphering geothermal resources in Deccan Trap region using electrical resistivity tomography technique. *Journal of the Geological Society of India*, *78*, 541-548.

[31]. Kana, J. D., Djongyang, N., Raïdandi, D., Nouck, P. N., & Dadjé, A. (2015). A review of geophysical methods for geothermal exploration. *Renewable and Sustainable Energy Reviews*, *44*, 87-95.

[32]. Rizzo, E., Giampaolo, V., Capozzoli, L., De Martino, G., Romano, G., Santilano, A., & Manzella, A. (2022). 3D deep geoelectrical exploration in the Larderello geothermal sites (Italy). *Physics of the Earth and Planetary Interiors*, *329*, 106906.

[33]. Passaro, S. (2010). Marine electrical resistivity tomography for shipwreck detection in very shallow water: a case study from Agropoli (Salerno, southern Italy). *Journal of Archaeological Science*, *37*(8), 1989-1998.

[34]. Zheng, W., Li, X., Lam, N., Wang, X., Liu, S., Yu, X., Sun, Z., & Yao, J. (2013). Applications of integrated geophysical method in archaeological surveys of the ancient Shu ruins. *Journal of archaeological science*, *40*(1), 166-75.

[35]. Simyrdanis, K., Papadopoulos, N., & Cantoro, G. (2016). Shallow off-shore archaeological prospection with 3-D electrical resistivity tomography: The case of Olous (modern Elounda), Greece. *Remote Sensing*, *8*(11), 897.

[36]. Gaber, A., Gemail, K. S., Kamel, A., Atia, H. M., & Ibrahim, A. (2021). Integration of 2D/3D ground penetrating radar and electrical resistivity tomography surveys as enhanced imaging of archaeological ruins: A case study in San El-Hager (Tanis) site, northeastern Nile Delta, Egypt. *Archaeological Prospection*, *28*(2), 251-267.

[37]. Tye, A. M., Kessler, H., Ambrose, K., Williams, J. D., Tragheim, D., Scheib, A., Raines, M., & Kuras, O. (2011). Using integrated near-surface geophysical surveys to aid mapping and interpretation of geology in an alluvial landscape within a 3D soil-geology framework. *Near Surface Geophysics*, *9*(1), 15-31.

[38]. Rucker, D. F., Noonan, G. E., & Greenwood, W. J. (2011). Electrical resistivity in support of geological mapping along the Panama Canal. *Engineering Geology*, *117*(1-2), 121-133.

[39]. Gouet, D. H., Meying, A., Ekoro Nkoungou, H. L., Assembe, S. P., Njandjock Nouck, P., & Ndougsa Mbarga, T. (2020). Typology of sounding curves and lithological 1D models of mineral prospecting and groundwater survey within crystalline basement rocks in the East of Cameroon (Central Africa) using electrical resistivity method and Koefoed computation method. *International journal of Geophysics*, *2020*, 1-23.

[40]. Junaid, M., Abdullah, R. A., Sa'ari, R., Ali, W., Rehman, H., Shah, K. S., & Sari, M. (2022). Water-saturated zone recognition using integrated 2D electrical resistivity tomography, borehole, and aerial photogrammetry in granite deposit, Malaysia. *Arabian Journal of Geosciences*, *15*(14), 1301.

[41]. Chambers, J. E., Meldrum, P. I., Wilkinson, P. B., Ward, W., Jackson, C., Matthews, B., Joel, P., Kuras, O., Bai, L., Uhlemann, S., & Gunn, D. (2015). Spatial monitoring of groundwater drawdown and rebound associated with quarry dewatering using automated time-lapse electrical resistivity tomography and distribution guided clustering. *Engineering Geology*, *193*, 412-420.

[42]. Saranya, T., & Saravanan, S. (2020). Groundwater potential zone mapping using analytical hierarchy process (AHP) and GIS for Kancheepuram District, Tamilnadu, India. *Modeling Earth Systems and Environment*, *6*(2), 1105-1122.

[43]. Subba Rao, N. (2006). Groundwater potential index in a crystalline terrain using remote sensing data. *Environmental geology*, *50*, 1067-1076.

[44]. Ibrahim-Bathis, K., & Ahmed, S. A. (2016). Geospatial technology for delineating groundwater potential zones in Doddahalla watershed of Chitradurga district, India. *The Egyptian Journal of Remote Sensing and Space Science*, *19*(2), 223-234.

[45]. Andualem, T. G., & Demeke, G. G. (2019). Groundwater potential assessment using GIS and remote sensing: A case study of Guna tana landscape, upper blue Nile Basin, Ethiopia. *Journal of Hydrology: Regional Studies*, *24*, 100610.

[46]. Tolche, A. D. (2021). Groundwater potential mapping using geospatial techniques: a case study of Dhungeta-Ramis sub-basin, Ethiopia. *Geology, Ecology, and Landscapes*, *5*(1), 65-80.

[47]. Adeyemo, I. A., Omosuyi, G. O., Ojo, B. T., & Adekunle, A. (2017). Groundwater potential evaluation in a typical Basement Complex environment using GRT index—a case study of Ipinsa-Okeodu area, near Akure, Nigeria. *Journal of Geoscience and Environment Protection*, *5*(03), 240.

[48]. Oni, T. E., Omosuyi, G. O., & Akinlalu, A. A. (2017). Groundwater vulnerability assessment using hydrogeologic and geoelectric layer susceptibility indexing at Igbara Oke, Southwestern Nigeria. *NRIAG Journal of Astronomy and Geophysics*, *6*(2), 452-458.

[49]. Shailaja, G., Gupta, G., Suneetha, N., & Laxminarayana, M. (2019). Assessment of aquifer zones and its protection via second-order geoelectric indices in parts of drought-prone region of Deccan Volcanic Province, Maharashtra, India. *Journal of Earth System Science*, *128*(4), 78.

[50]. Singh, S., & Tripura, J. (2022). Pumping test analysis for assessment of hydraulic parameters and aquifer system formation in hilly terrain. *Water Practice & Technology*, *17*(1), 492-501.

[51]. CGWB, (2022). Groundwater water year book, Himachal Pradesh. http://cgwb.gov.in/Regions/NHR/Reports/GWY%20BOOK%20HIMACHAL%20PRADESH%202021-2022.pdf. Accessed 02 May 2023.

[52]. CGWB, (2013). Ground water information booklet Hamirpur district, Himachal Pradesh. http://cgwb.gov.in/District_Profile/HP/Hamirpur.pdf. Accessed 18 July 2022.

[53]. Vasantrao, B. M., Bhaskarrao, P. J., Mukund, B. A., Baburao, G. R., & Narayan, P. S. (2017). Comparative study of Wenner and Schlumberger electrical resistivity method for groundwater investigation: a case study from Dhule district (M.S.), India. *Applied Water Science*, *7*, 4321–4340.

[54]. Suriyapor, P. (2020). 1-D Vertical Electrical Sounding (VES) Inversion with a lateral constraint (Doctoral dissertation, Department of Physics Faculty of Science, Mahidol University).

[55]. Okpoli, C. C. (2013). Sensitivity and resolution capacity of electrode configurations. *International Journal of Geophysics*, 2013.

[56]. Merrick, N. P. (1997). A new resolution index for resistivity electrode arrays. *Exploration Geophysics*, *28*(2), 106-109.

[57]. Eastern Research Group, Inc, & Center for Environmental Research Information (US). (1993). *Use of airborne, surface, and borehole geophysical techniques at contaminated sites: A reference guide*. US Environmental Protection Agency.

[58]. Samouëlian, A., Cousin, I., Tabbagh, A., Bruand, A., & Richard, G. (2005). Electrical resistivity survey in soil science: a review. *Soil & Tillage Research*, *83*, 173-193.

[59]. Orellana, E., & Mooney, H. M. (1966). Master tables and curves for vertical electrical sounding over layered structures. Interciencia, Madrid, 159 pp.

[60]. Bobachev, A. (2003). Resistivity sounding interpretation IPI2WIN version 3.0. 1. *Moscow State University, Moscow*.

[61]. Zohdy, A. A., Eaton, G. P., & Mabey, D. R. (1974). *Application of surface geophysics to ground-water investigations* (No. 02-D1). US Dept. of the Interior, Geological Survey: US Govt. Print. Off.

[62]. Tahama, K., Baride, A., Gupta, G., Erram, V. C., & Baride, M. V. (2022). Spatial variation of sub-surface heterogenieties within the dyke swarm of Nandurbar region, Maharashtra, India, for groundwater exploration using Inverse Distance Weighted technique. *HydroResearch*, *5*, 1-12.

[63]. Rahman, H. (2015). Spatial Distribution Analysis and Mapping of Groundwater Quality Parameters for the Sylhet City Corporation (SCC) Area Using GIS. *Hydrology*, *3*(1), 1.

[64]. Farid, H. U., Bakhsh, A., Ahmad, N., Ahmad, A., & Mahmood-Khan, Z. (2016). Delineating site-specific management zones for precision agriculture. *The Journal of Agricultural Science*, *154*(2), 273-286.

[65]. Bakhsh, A., Kanwar, R. S., & Malone, R. W. (2007). Role of landscape and hydrologic attributes in developing and interpreting yield clusters. *Geoderma*, *140*(3), 235-246.

[66]. Tran, B. Q., & Nguyen, T. T. (2008). Assessment of the influence of interpolation techniques on the accuracy of digital elevation model. *VNU Journal of Science Earth Sciences*, *24*, 176.

[67]. Ojo, E. O., Adelowo, A., Abdulkarim, H. M., & Dauda, A. K. (2015). A Probe into the Corrosivity Level and Aquifer Protective Capacity of the Main Campus of the University of Abuja, Nigeria: Using Resistivity Method. *Physics Journal*, *1*(2), 172.

[68]. Oladapo, M. I., Mohammed, M. Z., Adeoye, O. O., & Adetola, B. A. (2004). Geo-electrical investigation at Ondo State housing corporation estate, Ijapo, Akure, southwestern Nigeria. *Journal of Mining Geology*, *40*(1), 41–48.

[69]. Daniel, A., Louis, O., Emmanuel, C., & Kingsley, O. (2015). Delineation of potential groundwater zones using geoelectrical sounding data at Awka in Anambra State, South-eastern Nigeria. *European Journal of Biotechnology and Bioscience*, *3*(1), 01.

[70]. Emberga, T. T., Opara, A. I., Onyekuru, S. O., Omenikolo, A. I., Nkpuma, O. R., & Eluwa Nchedo, E. N. (2019). Regional hydrogeophysical study of the groundwater potentials of the Imo River Basin Southeastern Nigeria using surfcial resistivity data. *Australian Journal of Basic and Applied Sciences*, *13*(8), 76–94.

[71]. Niwas, S., & Singhal, D. C. (1985). Aquifer transmissivity of porous media from resistivity data. *Journal of Hydrology*, *82*(1-2), 143-153.

[72]. Niwas, S., & Singhal, D. C. (1981). Estimation of aquifer transmissivity from Dar-Zarrouk parameters in porous media. *Journal of hydrology*, *50*, 393-399.

[73]. Nwachukwu, S., Bello, R., & Balogun, A. O. (2019). Evaluation of groundwater potentials of Orogun, South–South part of Nigeria using electrical resistivity method. *Applied Water Science*, *9*(8), 184.

[74]. Oladapo, M. I., & Akintorinwa, O. J. (2007). Hydrogeophysical study of ogbese south western Nigeria. *Global journal of pure and applied sciences*, *13*(1), 55-61.

[75]. Henriet, J. P. (1976). Direct applications of the Dar Zarrouk parameters in ground water surveys. *Geophysical prospecting*, *24*(2), 344-353.

[76]. Youssef, M. A. S. (2020). Geoelectrical analysis for evaluating the aquifer hydraulic characteristics in Ain El-Soukhna area, West Gulf of Suez, Egypt. *NRIAG Journal of Astronomy and Geophysics*, *9*(1), 85-98.

بررسی هیدروژئوفیزیکی برای ارزیابی بودجه آب زیرزمینی و حفاظت از سفره‌های زیرزمینی در مناطق تپه‌ای

سونو سینگ[1*] ویجی شانکار[1] و جوزف تریپورا[2]

1. گروه مهندسی عمران، موسسه ملی فناوری حمیرپور، حمیرپور، هند

2. گروه مهندسی عمران، موسسه ملی فناوری پاتنا، پاتنا ، هند

ارسال 2023/03/09، پذیرش 2023/07/17

* نویسنده مسئول مکاتبات: sonu@nith.ac.in

چکیده:

ارزیابی پتانسیل آب زیرزمینی (GWP) و ظرفیت حفاظتی سفره‌های زیرزمینی برای ارائه راه‌حل‌هایی برای چالش‌های اکتشاف آبخوان و شرایط در مناطق تپه‌ای ضروری است. این مطالعه در منطقه تپه‌ای Hamirpur، هیماچال پرادش، هند، برای به دست آوردن داده‌های صدای الکتریکی عمودی یک بعدی (VES) برای اکتشاف آب‌های زیرزمینی و ارزیابی آسیب‌پذیری زیرلایه‌ها انجام شد. چهل سایت VES در پیکربندی الکترود شلمبرگر استفاده شد. تجزیه و تحلیل داده‌ها منجر به 2-5 منحنی طبقه‌بندی شده مختلف شد. با توجه به مقاطع ژئوالکتریک، دو تا پنج لایه خاک در زیر منطقه وجود دارد، یعنی شیل / خاک رس (10-650 اهم متر)، ماسه سنگ شکسته / شن / ماسه (10,3-436 اهم متر)، خاک رس مخلوط شن / خاک رس. مخلوط ماسه / ماسه سنگ دانه درشت (1,06-355 اهم متر)، کنگلومرا / رس / ماسه سنگ سخت (60,5-658,7 اهم متر)، ماسه سنگ / شیل (90,8-125 اهم متر) با مقاومت آبخوان (AR) در پرانتز. نقشه‌های توزیع مقاومت آبخوان (AR)، هدایت طولی (S)، ضخامت لایه (LT) و مقاومت عرضی (TR) با استفاده از داده‌های تفسیر شده VES برای لایه‌های فرعی مختلف با استفاده از ArcGIS 10.1 تولید شد. لایه‌های زیرسطحی دوم و سوم زمین‌شناسی عموماً متخلخل و نفوذپذیر هستند. مقادیر S برای لایه‌های زیرین معمولاً کمتر از یکپارچگی است که نشان‌دهنده مناطق آسیب‌پذیر با خطر آلودگی قابل‌توجه است. بر اساس مقادیر S، اقشار به پنج دسته ضعیف (5/55 درصد)، ضعیف (19/43 درصد)، متوسط (19/45 درصد)، خوب (38/89 درصد) و خیلی خوب (16/68 درصد) تقسیم می‌شوند. مناطقی با ظرفیت حفاظتی متوسط تا خیلی خوب به عنوان مناطقی با GWP بالا برنامه ریزی شده‌اند. نتایج مطالعه در کنترل اولیه آلودگی و ارزیابی برای مدیریت پایدار آب‌های زیرزمینی مفید است.